Aerospace Science and Technology 58 (2016) 418–426

Contents lists available at ScienceDirect

Aerospace Science and Technology

www.elsevier.com/locate/aescte

A UWB positioning network enabling unmanned aircraft systems auto land

Euiho Kim [a,*], Dongkyu Choi [b]

[a] Department of Aeronautical and Mechanical Engineering, Cheongju University, South Korea
[b] Department of Aerospace Engineering, University of Kansas, Lawerence, KS, 66045 USA

ARTICLE INFO

Article history:
Received 25 February 2016
Received in revised form 25 July 2016
Accepted 6 September 2016
Available online 14 September 2016

Keywords:
Unmanned aerial vehicles
Ultra wide band technology
Aircraft navigation
Global positioning system

ABSTRACT

Although Unmanned Aircraft Systems (UAS) have become popular, the auto land of a fixed wing UAS has still remained as a significant challenge. This paper presents a UAS auto landing system based on a Ultra Wide Band (UWB) positioning network. The geometry of the UWB anchors in the network is optimized to provide precise positioning accuracy during the course of UAS landing. The notable performance characteristics of the system is that the positioning of the UAS becomes more accurate as it approaches to the runway more closely. At the point of a landing flare, the landing system is expected to provide vertical positioning accuracy better than 20 cm in 95 percent of time. The paper discusses the methodology of designing the proposed UWB positioning network architecture and the positioning performance analysis through simulations.

1. Introduction

The Unmanned Aircraft Systems (UAS) have become widely popular and their applications are not only limited to military operations but also include various civil applications such as crop monitoring, aerial mapping, and aerial photos [1–3]. It is also expected that the UAS will be an important part of future air transportation systems [4]. However, one of the biggest challenges to the widespread of the UAS in the National Airspace System (NAS) is safety. Particularly, the autonomous landing of a fixed wing UAS is still problematic and its safety must be ensured before the introduction of the UAS into the NAS.

For manned aircraft, the Instrument Landing System (ILS) has been used as a primary landing system in the world [5]. More recently, the Ground Based Augmentation System (GBAS) of Global Positioning System (GPS) is being introduced and expected to replace ILS [6,7]. These two systems have not been seriously considered as the auto landing system for a small fixed wing UAS. The primary reasons could be significant costs associated with the ground equipment and avionics. In addition, their positioning accuracy, particularly in vertical, does not seem to be sufficient. A reported vertical positioning accuracy of the state-of-the-art GBAS system is around 1 m in 95 percents of time [8]. For a relatively larger aircraft such as commercial manned jets, the GBAS positioning accuracy should be satisfactory. However, the smaller fixed wing UAS whose height is less than 1 m or so, a reliable auto landing would not be ensured even when the GBAS properly operates.

For small fixed-wing UAS, there have been many kinds of vision-based auto landing approaches [9–15]. Those approaches can be classified as onboard-based [9–11] or ground-based systems [12–15]. In Reference [9], a UAS has a gimbaled camera, GPS, and an inertial measurement unit (IMU). The GPS position guides a UAS to a nearby runway, then camera images with IMU readings are processed to detect a runway and to extract the UAS position relative to the runway during the landing operation. Reference [10] takes a similar approach as reference [9], but it utilizes runway light fixtures to find headings and position of a UAS relative to the runway. For the cases of emergency, such engine failures, reference [11] developed a machine learning-based image processing algorithms that search for nearby flat surfaces appropriate for a landing. However, no precise positioning is given during the landing operation in this approach. In the ground-based systems [12–15], cameras with image processing algorithms detect a UAS, compute its relative bearing and position, and send the information to the approaching UAS for an auto landing. The vision-based auto lands could be a promising solution for a fixed wing UAS. However, the performance and reliability of the proposed image processing algorithms under various lighting conditions should be further confirmed.

Instead of a vision, some other approaches use a code-based differential GPS, a tracking radar, or LIDAR [16–19]. Reference [16] used a code-based differential GPS and a barometric altimeter for the autonomous landing of a small UAS to a ship. Due to the

* Corresponding author.
E-mail addresses: euihokim@cju.ac.kr (E. Kim), dongkyu.choi@ku.edu (D. Choi).

http://dx.doi.org/10.1016/j.ast.2016.09.005
1270-9638/

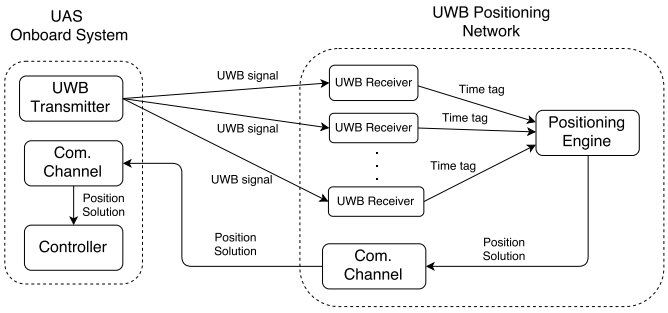

Fig. 1. Interaction between the UAS onboard system and the UWB positioning network.

lack of precision, the proposed approach brings a UAS to a large net standing on the ship surface instead of a soft landing. Reference [17] integrated a code-based differential GPS with a precision tracking radar. The precision tracking radar provides more precise position of a UAS than the differential GPS within 2 miles from the runway touch point. Therefore, a UAS uses the differential GPS to reach up to 2 miles from the runway touch point and switches its primary navigation source to the precision tracking radar-based position during the remaining landing procedures. This approach is more appropriate for a large military UAS that is equipped with the transceiver for the precision tracking radar. References [18] and [19] use a 3D LIDAR with IMU to detect obstacles, select and map a possible landing zone, and perform an auto landing. Because of the large form factor of a 3D LIDAR and its weight, these approaches are suited for a relative large UAS.

This paper introduces a novel passive Ultra Wide Band (UWB) positioning network for a fixed-wing UAS landing system. The conceptual operation of the UWB positioning during a landing is depicted in Fig. 1. In this proposed landing system, the passive UWB positioning network listens to the UWB signals emitted from the UAS. In this way, the UWB positioning network minimizes required UWB communications and does not interrupt Radio Frequency (RF) environment in an airport. The position of the UAS is computed on the ground by using the received UWB signals at the anchors and is sent back to the UAS through a protected aviation communication channel. The most important advantage of the proposed UWB auto landing system is that the vertical positioning accuracy would be superior to the any of the prior arts by taking advantage of the centimeter-level of the UWB ranging capability and the optimized anchor network geometry for a landing. Nonetheless, the onboard equipment requirements and computational load of a UAS are very minimal.

This paper first overviews the principles of UWB positioning and positioning uncertainty in Section 2. Section 3 discusses modeled landing path configurations and the associated vertical positioning accuracy during the course of landing. Section 4 introduces the methods used to search for the optimal geometry of the UWB positioning network. Section 5 presents the resultant optimal UWB network that enables a UAS auto land and its performance analysis. Conclusions will be followed in Section 6.

2. Overview of UWB positioning network

2.1. Overview of ultra wide band

The Ultra Wide Band (UWB) for ranging operates in the frequency bands from 3.1 to 10.6 GHz. This wide band frequency allows extremely sharp pulse widths from a few hundred pico seconds to nano seconds [20,21]. Using the sharp UWB pulses, it is possible to obtain precise ranging measurements within centimeter-level of accuracy. Because of the precise ranging accuracy and the wall penetration capability of the UWB, the UWB is increasingly popular for navigation and tracking in indoor and outdoor.

A UWB positioning system consists of a user tag and several anchors fixed at known coordinates. In a passive or tracking mode, the anchors are time-synchronized and one of the anchors or a master station gathers the time stamps of the received signals from other anchors. The master station formulates time difference of arrival (TDOA) measurements to compute the user position and sends back the computed position to the user. Note the time duration from the computation of the position solution to the delivery of the solution to the user must be minimal for a high dynamic user. In this passive mode, the time synchronization accuracy among the anchors is critical in the tracking mode. In a wired network using an optical fiber and a dedicated FPGA, the time synchronization can be maintained under 100 picoseconds [22,23], whose impact to a positioning accuracy is insignificant in most applications. A time synchronization in a wireless network is much more challenging, where the achievable precision of the time synchronization used to be about 10 μs [24]. However, recent research has reported a few nano seconds time synchronization performance by taking advantage of recent hardware advancements [25].

In an active positioning mode, on the other hand, the distance between a tag and an anchor is measured through a two-way communication. The coordinates of the anchors are usually embedded in communication messages. When the user receives range measurements from more than 2 or 3 anchors, it computes its positing through Time of Arrival (TOA) formulation. Note that the time synchronization error is eliminated in this approach, but the two-way communications require the hardwares of the tag and anchors to be more sophisticated than the tracking mode.

The UWB positioning approach employed in this paper is the passive tracking mode. The main motivation in using the passive mode is to reduce UWB communications between a tag (aircraft) and anchors such that any interference effects on other aviation navigation instruments can be minimized in an airport environment. However, the active positioning can also be used if the environmental limitation is not a concern.

2.2. TDOA positioning uncertainty analysis

This section briefly discusses the TDOA positioning uncertainty analysis in the passive navigation mode.

Let us assume that there are m anchors in a UWB positioning network and the time synchronization between anchors are maintained under sub-nano (wired) or a few nano (wireless) seconds as discussed before. The coordinate of the ith anchor is denoted as $\boldsymbol{a}_i = (a_{i,x}, a_{i,y}, a_{i,z})$. Taking $\boldsymbol{a}_1$ as the reference node, a user location, $\boldsymbol{x}_u$, can be computed from

$$\delta\hat{\boldsymbol{x}}_u = (\boldsymbol{H}^\top \boldsymbol{W}\boldsymbol{H})^{-1}\boldsymbol{H}^\top \boldsymbol{W} \tag{1}$$

where $\boldsymbol{W}$ is a weighting matrix and $\boldsymbol{H}$ matrix is [26]

$$\boldsymbol{H} = \begin{bmatrix} \dfrac{\boldsymbol{x}_u - \boldsymbol{a}_2}{\|\boldsymbol{x}_u - \boldsymbol{a}_2\|} - \dfrac{\boldsymbol{x}_u - \boldsymbol{a}_1}{\|\boldsymbol{x}_u - \boldsymbol{a}_1\|} \\ \dfrac{\boldsymbol{x}_u - \boldsymbol{a}_3}{\|\boldsymbol{x}_u - \boldsymbol{a}_3\|} - \dfrac{\boldsymbol{x}_u - \boldsymbol{a}_1}{\|\boldsymbol{x}_u - \boldsymbol{a}_1\|} \\ \vdots \\ \dfrac{\boldsymbol{x}_u - \boldsymbol{a}_m}{\|\boldsymbol{x}_u - \boldsymbol{a}_m\|} - \dfrac{\boldsymbol{x}_u - \boldsymbol{a}_1}{\|\boldsymbol{x}_u - \boldsymbol{a}_1\|} \end{bmatrix}. \tag{2}$$

It is assumed that the range measurement error at ith receiver follows a Gaussian distribution with zero mean and the standard deviation of σ_{ϵ_i}. Then, the position error standard deviation as σ_p has the following forms

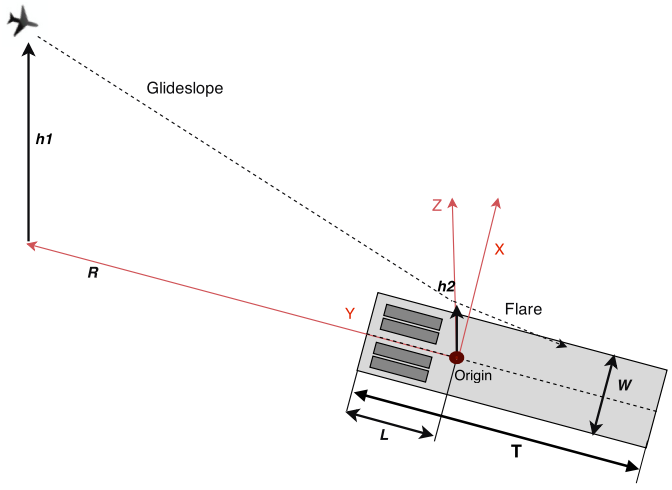

Fig. 2. A modeled runway configuration and landing path.

$$\sigma_p = \sqrt{\text{trace}(\boldsymbol{H}^\top \boldsymbol{W} \boldsymbol{H})^{-1}} \tag{3}$$

where the weighting matrix $\boldsymbol{W}$ is

$$\boldsymbol{W} = \begin{bmatrix} \sigma_{\epsilon_1}^2 + \sigma_{\epsilon_2}^2 & \sigma_{\epsilon_1}^2 & \cdots & \sigma_{\epsilon_1}^2 \\ \sigma_{\epsilon_1}^2 & \sigma_{\epsilon_1}^2 + \sigma_{\epsilon_3}^2 & \cdots & \sigma_{\epsilon_1}^2 \\ \vdots & \vdots & \ddots & \vdots \\ \sigma_{\epsilon_1}^2 & \sigma_{\epsilon_1}^2 & \cdots & \sigma_{\epsilon_1}^2 + \sigma_{\epsilon_m}^2 \end{bmatrix}^{-1} \tag{4}$$

The positioning accuracy of a user in the UWB positioning network will be evaluated by using Eq. (3).

3. Parameters for the design of a UAS auto land system

3.1. Runway configuration and landing path

Fig. 2 depicts the runway configuration taken in this paper. From the origin of the local Cartesian coordinate on the runway, the aircraft glideslope begins at the range of R and at the height of $h1$. At the height of $h2$ above the origin, the nose of aircraft is raised and the landing flare begins. Then the touchdown and roll-out phases are followed. L is the length from the front end of the runway to the origin. T is the total length of the runway and W is the width. Following the typical configurations of a small municipal airport, L, T, and W are set to 50 m, 2000 m, and 30 m, respectively.

The range of today's UWB device can extend to around 350 m without any blockages. For this reason, R is set to 300 m. The height of the flare point, $h2$, is set to 50 cm in this paper because most UAS are expected to successfully finish a landing from this height by just gliding. It is possible that many UAS may need to take different glideslopes during a landing, depending on their form factor and maneuverability. Considering the landing capability of various UAS and UWB Radio Frequency (RF) coverage, the range of glideslopes is set to between 5 degrees and 13 degrees, which will yield in $h1$ up to 69.5 m. Note that the runway geometry and the glideslopes may change depending on an airport environment and the coverage of UWB devices.

3.2. Required positioning accuracy

Assuming that no large objects are present along the course of a landing path, the usual threat during a landing is the collision to the ground. Thus, the vertical positioning accuracy of an aircraft landing system is particularly important. Therefore, the key parameter in determining the required positioning accuracy is the ratio

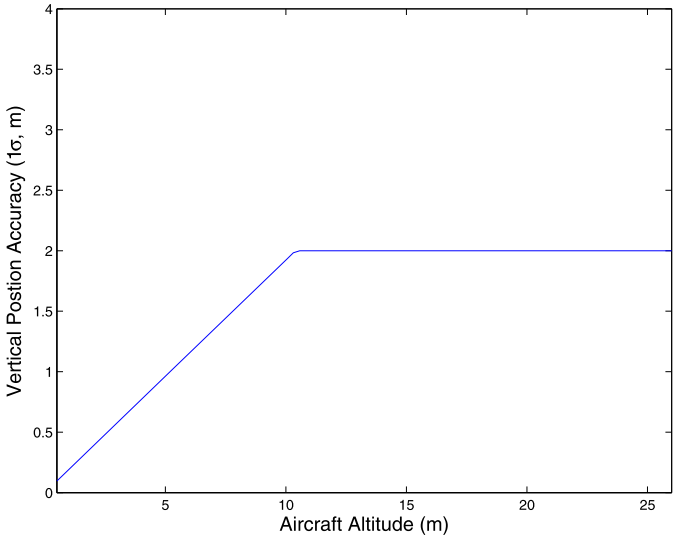

Fig. 3. Required vertical positioning accuracy during the modeled UAS landing.

between an aircraft altitude Above Ground Level (AGL) and a vertical positioning accuracy (VPA, 1σ), which is defined as Vertical Protection Ratio (VPR). Then, the VPR can be formulated as follows,

$$\begin{aligned} VPR(y, GS) &= \frac{AGL}{VPA} \\ &= \frac{h2 + y/tan(GS)}{VPA} \end{aligned} \tag{5}$$

where y is the distance in the Y axis and GS is a glideslope angle. Note that the VPR must be large enough in all y values that the probability of hitting the ground before the flare point is kept very small. In this paper, VPR is set to 5.2 such that the probability of having a position error beyond 5.2 σ away from the true position is less than 2×10^{-7}, assuming that the vertical positioning error can be modeled as a zero mean Gaussian distribution. In other words, the probability that a positioning error could cause aircraft to collide with the ground before the flare point is less than 2×10^{-7}. This level of safety is required in ILS and GBAS [27,28]. However, note that the entire risk is allocated to the positioning error in this conceptual design. Further risk analysis and allocations will be performed in a future work.

Fig. 3 shows the proposed VPA requirement (1σ) with respect to the aircraft AGL during the descent. Note that, the required VPA is as high as 9.6 cm at the height of $h2$ and is truncated to 2 m when the AGL is larger than 10.3 m to avoid large vertical positioning errors.

Note that the horizontal positioning accuracies in the X and Y axes are also important. But, it was found that the horizontal accuracy is usually sufficient when the a UWB positioning network meets the VPR. Therefore, the horizontal positioning accuracy does not play an important role in designing a positioning network.

In this paper, it is assumed that the UWB range error characteristics have a zero mean and a standard deviation of 5 cm with a Gaussian distribution [29,20]. The range error includes the error source of time synchronization, thermal noise, multipath, and surveyed anchor coordinates.

4. UWB positioning network architectures

In this work, it is assumed that the UAS can leverage GPS to get to the coverage of the proposed UWB landing system. When the UAS detects UWB signals, the UWB-based positioning becomes a primary navigation source. And, the GPS-based positioning will

run in a background mode. Note that the UWB positioning is performed with respect to the runway coordinates. And, the transformation between the GPS WGS 84 and the runway coordinates will be needed for a seamless landing operation. If the origin of the runway coordinates is surveyed in the WGS 84 coordinate system, the transformation between the two coordinates can be easily performed.

For the development of the UWB positioning network, the locations of the anchor nodes must be determined. The factors in determining the anchor nodes are the required UAS positioning accuracy along landing paths, RF range of UWB devices, and runway configurations. This section first overviews the ranging source optimization algorithm and introduces the proposed approaches to design the UWB anchor node geometry.

4.1. Overview of optimal ranging source location algorithm

The algorithms presented in this paper search for the set of anchor node geometries meeting the required positioning accuracy with the minimum number of anchors. The baseline search engine for the network is Binary Integer Linear Programming (BILP) [30]. To avoid an exhaustive search, the BILP also uses various heuristics such as distances between anchors, the number of difference of the anchors on the ground and in the air, and the symmetry of anchor locations with respect to the runway.

The BILP can be formulated as below and searches for an optimal UWB anchor placement through iterations.

$$\begin{aligned} \text{minimize } & Z = \sum_{i=1}^{N} w_i p_i = \boldsymbol{w}^\top \boldsymbol{p} \\ \text{subject to: } & \boldsymbol{V}\boldsymbol{p} \geq \boldsymbol{v} \\ & \boldsymbol{D}\boldsymbol{p} \leq \boldsymbol{d} \\ & \boldsymbol{A}\boldsymbol{p} \leq \boldsymbol{a} \\ & \boldsymbol{S}\boldsymbol{p} \leq \boldsymbol{s} \\ & (\boldsymbol{t}-\boldsymbol{b})^\top \boldsymbol{p} \leq k \\ & \boldsymbol{w}^\top \boldsymbol{p} \leq Z_{min} \\ & \mathbf{1}^\top \boldsymbol{p} \leq N_{min} \\ & p_i \in \{0,1\} \end{aligned} \tag{6}$$

where Z is the cost function to be minimized and $\boldsymbol{p}$ is the grid index column vector of the candidate anchor locations. $\boldsymbol{p}$ takes the binary value of either 0 or 1. When $p_i = 1$, it contains an anchor at the ith anchor location. Otherwise, $p_i = 0$. The vector $\boldsymbol{w}$ is a weighting factor on $\boldsymbol{p}$ that assigns preference of an anchor location to another. In this paper, there is no preference on any anchors. Therefore, $\boldsymbol{w}$ is set to $\mathbf{1}$. N is the total number of the candidate anchor locations.

The matrix $\boldsymbol{V}$ in Eq. (6) is a visibility matrix. The ith row of $\boldsymbol{V}$ corresponds to a grid index of a user location and the jth column to an anchor location. The elements of the matrix $\boldsymbol{V}$ also take on the value of either 0 or 1. If a user at the ith row location has a line of sight to the anchor at the jth column location, $\boldsymbol{V}_{ij}$ is equal to 1. Otherwise, $\boldsymbol{V}_{ij}$ is equal to 0. The vector $\boldsymbol{v}$ is the required minimum number of visible anchors at the corresponding user location and is set to 5 in this paper. Because a UAS should see 5 or more anchors to meet the proposed positioning accuracy during a landing, this constraint would help to narrow down the search space of the possible anchor networks. However, the vector $\boldsymbol{v}$ can be as low as 4 in the passive tracking mode of a UWB operation.

The matrix $\boldsymbol{D}$ and the vector $\boldsymbol{d}$ set the limit on the separation between anchors. If the distance between i and j anchors is less than the minimum separation, $\boldsymbol{D}_{ij}$ is equal to 0. The vector $\boldsymbol{d}$ is a vector of $\mathbf{1}$s that does not allow any anchors within the minimum separation distance. The minimum separation distance ranges from 5 m to 10 m in this paper.

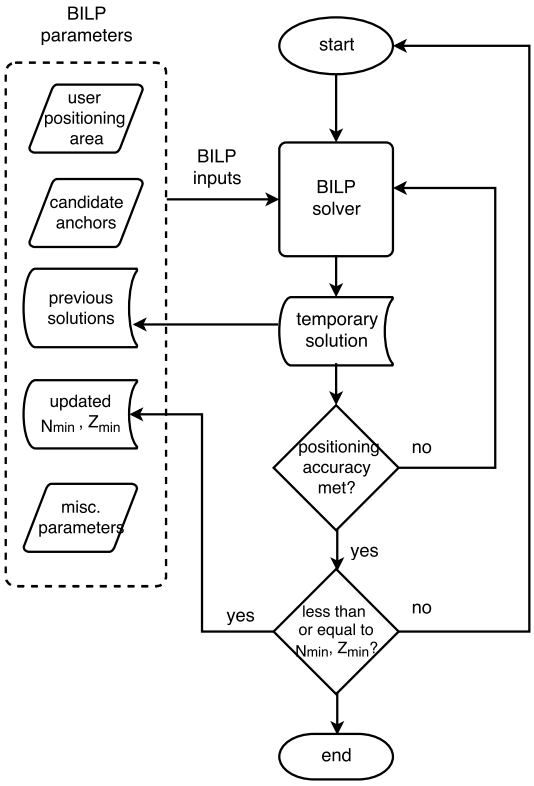

Fig. 4. The flowchart describes the overall iterative optimization procedures using BILP.

The matrix $\boldsymbol{A}$ contains the previous solution sets denoted as $\boldsymbol{p}_s$ at each row, and the vector $\boldsymbol{a} = (\boldsymbol{p}_s^\top \mathbf{1} - u)\mathbf{1}$ forces the BILP formulation to yield a unique solution during the iterative search. u is a non-zero positive integer number and is set to 2 in this paper.

The matrix $\boldsymbol{S}$ is a symmetric matrix. S_{ii} is equal to 1 and S_{ij} is set to -1 if ith and jth anchors are symmetrically located with respect to the runway coordinates. The vector $\boldsymbol{s}$ is zero vectors. This constraint enforces a symmetric positioning accuracy in the user positioning spaces.

The vectors $\boldsymbol{t}$ and $\boldsymbol{b}$ indicate whether an anchor is located on or above the ground. If t_i is equal to 1, the ith anchor is located above the ground. Otherwise, t_i is equal to zero. Likewise, if b_i is equal to 1, the ith anchor is located on the ground. Otherwise, b_i is equal to zero. k is the difference between the number of anchors located on the air and on the ground and is set to 2 in this paper.

Z_{min} is the minimum cost among the valid solution sets found through previous iterations. Similarly, N_{min} is the minimum number of anchors among the valid solution sets found through previous iterations. Z_{min} and N_{min} can be initially set to a large number. Whenever, a valid anchor network geometry is found, Z_{min} and N_{min} are updated to the lowest values found during the iteration. Eq. (6) is solved by using an open source GNU Linear Programming Kit [31].

Fig. 4 illustrates the overall optimization procedure using the BILP when implemented in a software. With the input parameters, the BILP solver outputs a temporary and valid anchor set that meets all of the constraints. Then, the user positioning accuracy over the landing path is inspected to check if the positioning accuracy requirement is met in all of the user positioning area or landing paths with the given anchor geometry. If not, the BILP re-

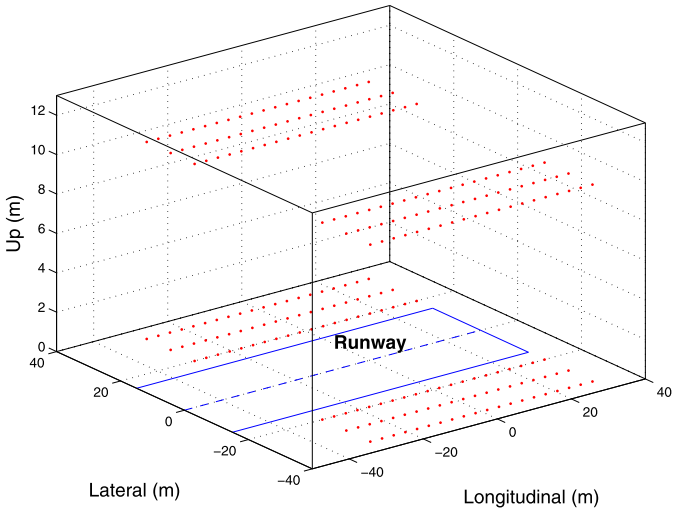

Fig. 5. Candidate anchor locations to support UAS landing.

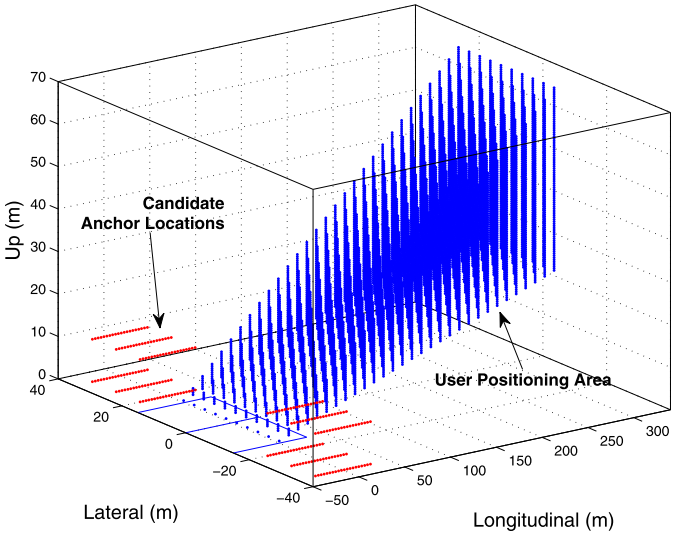

Fig. 6. Positioning service area to support UAS landing.

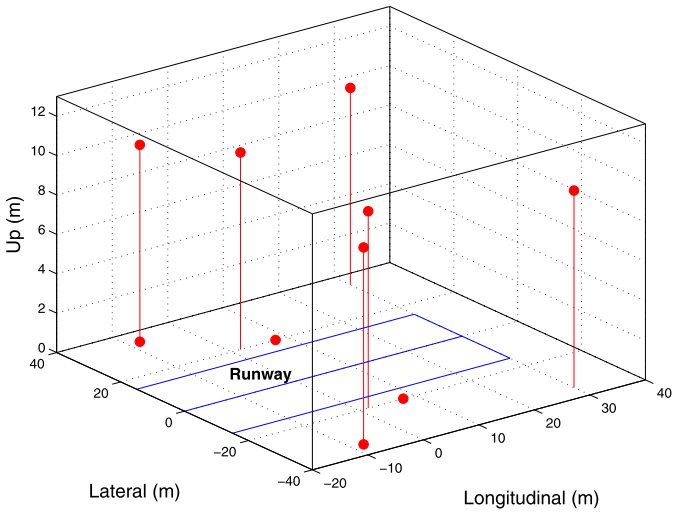

Fig. 7. Resultant ten anchor locations (red circles) from the optimal anchor location algorithms. (For interpretation of the references to color in this figure legend, the reader is referred to the web version of this article.)

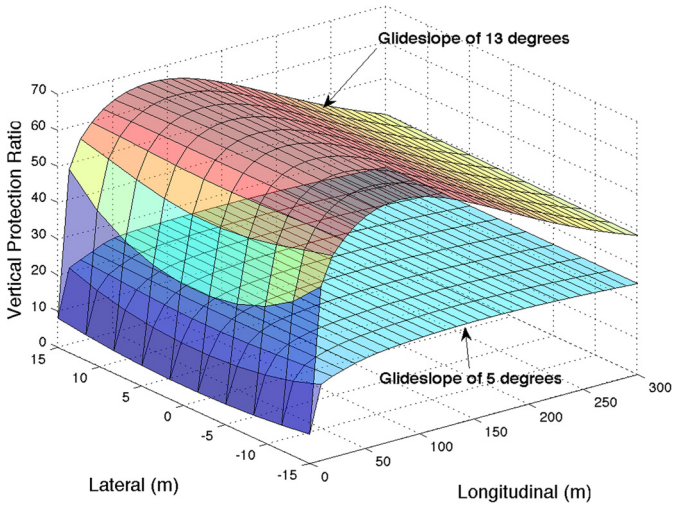

Fig. 8. The ratio of aircraft altitude (AGL) to vertical positioning error (VPE).

peatedly places additional anchors until the positioning accuracy is met or the values of Z_{min} or N_{min} are exceeded. This process is iterated while updating the BILP parameters. When the BILP solver outputs no solutions in tens of iterations, a (local) optimal solution is considered to be found and the execution of the optimization process is terminated.

4.2. Candidate anchor locations and positioning service area

Fig. 5 shows the array of candidate anchor locations around the runway. There are two anchor locations separated by 7.5 m in the lateral directions at each side of the runway. In the longitudinal direction, there are 20 anchors separated by 3 meter. In the vertical direction, the anchors are either located on the ground or at 10 m height antennas. Therefore, there are a total of 240 possible anchor locations.

Fig. 6 shows the UAS positioning service area during the landing operation. The lateral span of the positioning service area is 30 m that is the width of the runway. The longitudinal range is up to 300 m from the origin of the local runway coordinates. The maximum and the minimum slopes of the user positioning service area correspond to the supported glideslopes of 5 and 13 degrees. Note that the RF coverage of the UWB positioning network is much larger and positioning would be possible in the RF coverage where a UAS may have line of sights to multiple anchors. However, only the user positioning area guarantees the required VPR.

5. Resultant optimized UWB positioning network

This section presents the resultant anchor locations based on the candidate anchor locations and user positioning area. The positioning performance of the anchor network is also analyzed.

5.1. Resultant baseline anchor locations

Fig. 7 shows the resultant optimal anchor geometry from iteratively solving Eq. (6). Six of the anchors are located in 10 meter height antennas and the rest of them are placed on the ground. As shown in Fig. 7, the anchor geometry is symmetric with respect to the runway. In the anchor location search algorithms, the VPR is required to be larger than 5.22. Fig. 8 shows that the resultant VPR is overall much larger than 5.22 and the minimum VPR of 5.22 exists at the flare or origin point.

Figs. 9, 10, and 11 show the superimposed theoretical positioning accuracy (1σ) of the landing paths in the maximum and the minimum glideslopes. Because the resultant anchor geometry

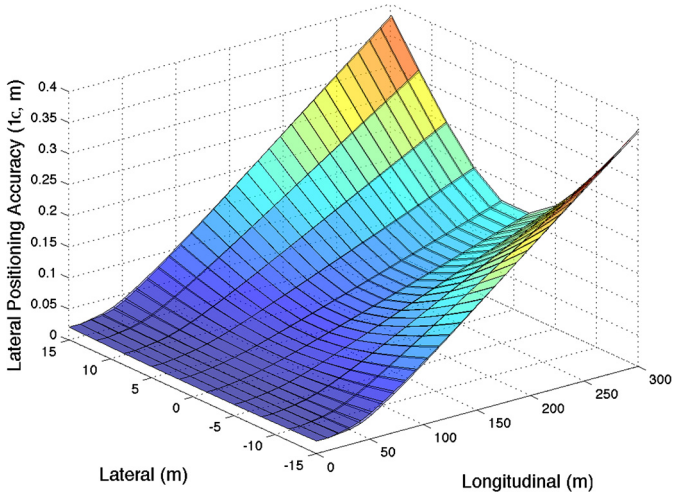

Fig. 9. Theoretical positioning accuracy (1σ) in the lateral direction.

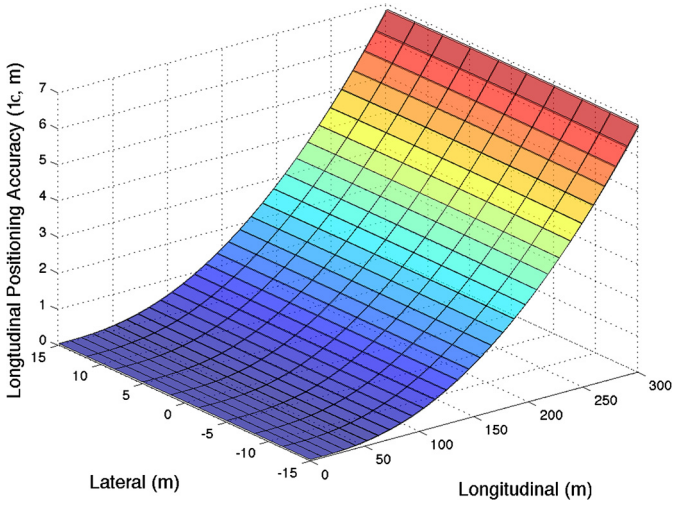

Fig. 11. Theoretical positioning accuracy (1σ) in the longitudinal direction.

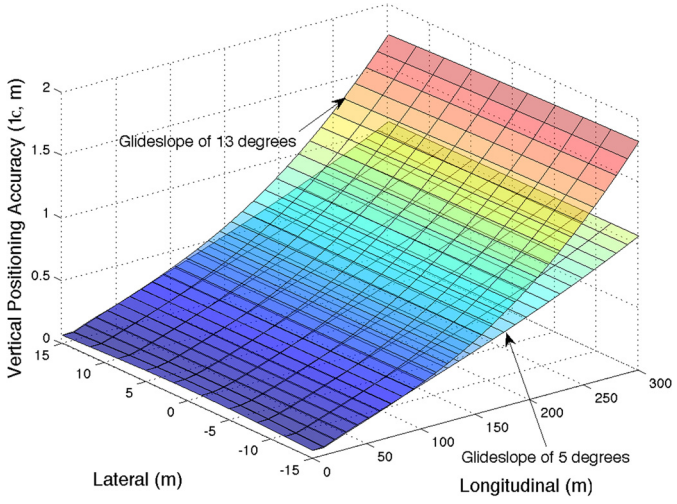

Fig. 10. Theoretical positioning accuracy (1σ) in the vertical direction.

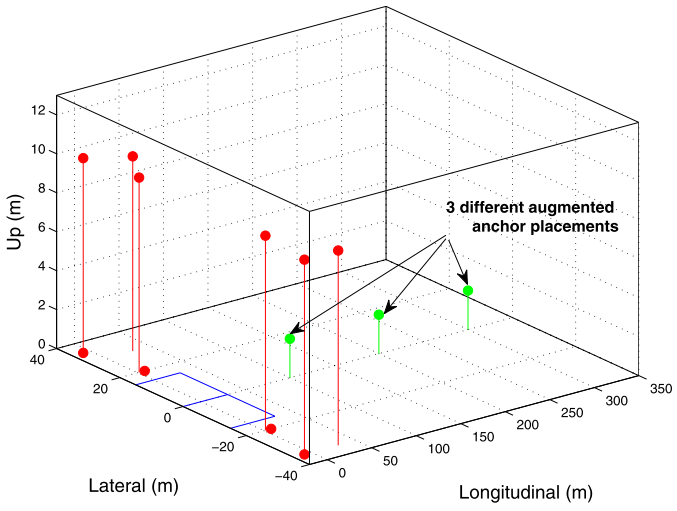

Fig. 12. Three augmented anchor locations to improve positioning accuracy in the longitudinal direction.

is symmetric, the positioning accuracy during the landing is also symmetric. In Fig. 11, the lateral positioning accuracy is better than 40 cm (1σ). Note that the lateral accuracy does not significantly vary with respect to glideslope changes. In Fig. 10, the vertical accuracy is as good as 9 cm (1σ) at the flare point and degrades as the longitudinal range increases from 0 to 300 m. The glideslope of 5 degrees provides a slightly better vertical positioning accuracy than the glideslope of 13 degrees. And, the vertical positioning accuracy of the landing paths between those glideslopes locates inside the two extremes. Therefore, the UAS landing with the glideslopes from 5 to 13 degrees is well supported in the lateral and vertical directions.

The longitudinal positioning accuracy shown in Fig. 11 also overall seems to be sufficient to support an auto landing. However, the longitudinal positioning accuracy is somewhat poor where the longitudinal range is larger than 200 m. The reason is that the anchors are clustered in one direction at the UAS point of view, therefore the Dilution of Precision of the anchor geometry is particularly bad in the region. If a UAS can use other onboard sensors such as Inertial measurement units (IMU) for the longitudinal velocity, then a simple Kalman filer would enhance the longitudinal positioning accuracy. Alternatively, additional anchors could be placed to improve the longitudinal positioning accuracy, which is further discussed in the next subsection.

5.2. Augmented anchor geometry for the longitudinal direction

Considering the limited space and safety in an airport, the candidate anchor locations were designated near the runway as shown in Fig. 5. However, if it is possible to place additional anchors in front of the runway, that will further improve the longitudinal accuracy as a result of the better angular diversity between the UAS and the anchors in the longitudinal direction. And, the augmented anchors should be located along the Y axis to keep the symmetry of the positioning accuracy of the network.

To see the benefit of an augmented anchor, the following three cases are examined. The first case places an additional anchor at $(0, 100, 2)$, the second case at $(0, 200, 2)$, and the third case at $(0, 300, 2)$ in the runway coordinates. The height of the augmented anchors is set to 2 meters to avoid a tall structure below the landing path. Fig. 12 shows the three cases of the augmented anchors along the Y axis. And, Fig. 13, Fig. 14, and Fig. 15 show the corresponding longitudinal positioning accuracy for each case, respectively. In the figures, the improvement of the longitudinal accuracies start being clearly seen when the UAS passes through the augmented anchors. Among the three cases, a dramatic improvement is obtained from the third case in Fig. 15, whose longitudinal positioning accuracy is 3 cm (1σ) at the flare point and 1 m (1σ) at the initial descending point.

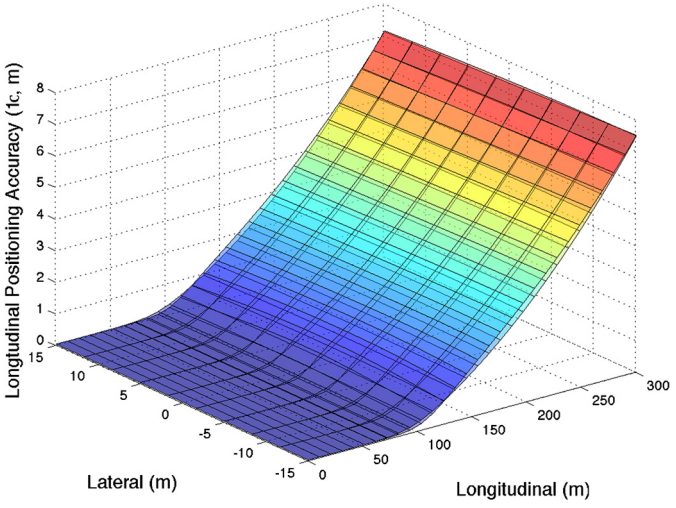

Fig. 13. Improved longitudinal positioning accuracy from using the augmented UWB anchor network placed at $(0, 100, 2)$. There is little difference in the positioning accuracy between the two glideslopes.

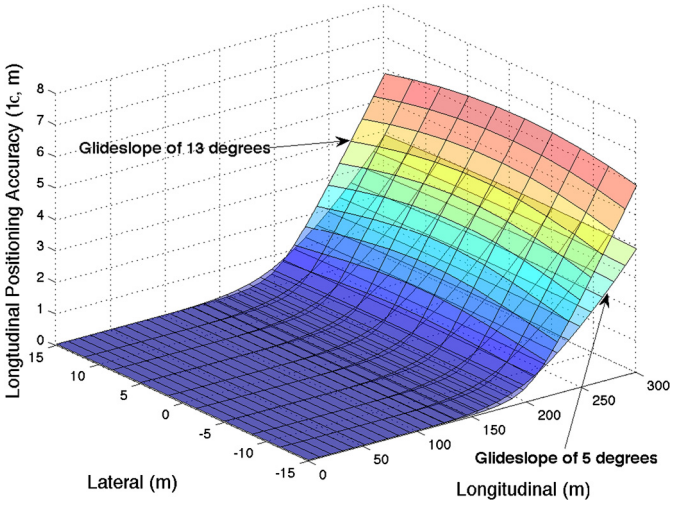

Fig. 14. Improved longitudinal positioning accuracy from using the augmented UWB anchor network placed at $(0, 200, 2)$.

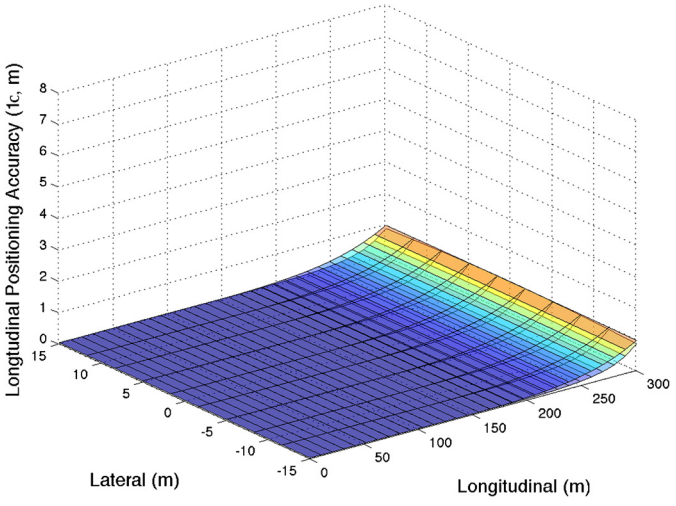

Fig. 15. Improved longitudinal positioning accuracy from using the augmented UWB anchor network placed at $(0, 300, 2)$. There is little difference in the positioning accuracy between the two glideslopes.

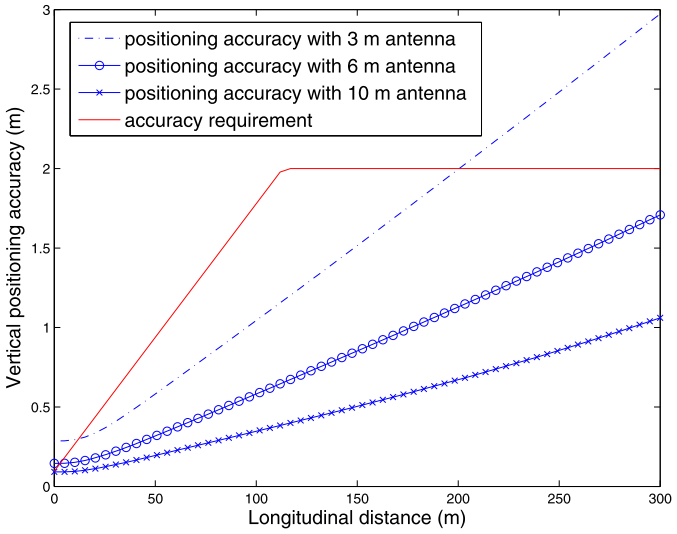

Fig. 16. The vertical positioning accuracies using 3 m, 6 m, and 10 m height antennas are compared with the vertical accuracy requirement. The positioning accuracy is evaluated by following the landing path of 5 degrees glideslope.

5.3. Impacts of antenna heights on the vertical positioning accuracy

In this particular problem, the user-to-ranging source geometry as well as the required vertical positioning accuracy dramatically change as the UAS approaches to the runway. To analyze the impact of an antenna height for this problem, the obtainable vertical positioning accuracy along the landing path of the 5 degrees glideslope is computed while applying different antenna heights from 10 m to the optimal anchor network in Fig. 7. Fig. 16 compares the obtainable vertical positioning accuracies using 3 m, 6 m, and 10 m height antennas with the proposed vertical accuracy requirement in Fig. 3. Note that the anchor network with the 6 m height antenna can still meet the accuracy requirement in most of the landing paths except for the flare point region. Near the flare point, the vertical positioning accuracy with the 6 m height antenna exceeds the accuracy requirement by about 6 cm. Therefore, some relaxation of the proposed vertical accuracy requirement would allow the use of the antenna heights lower than 10 m.

While keeping the same vertical positioning accuracy requirement, an alternative optimal anchor network can be found using antenna heights other than 10 m. However, when an antenna height is low, it will increase the required number of anchors in a network. Fig. 17 and Fig. 18 show the alternative optimal anchor networks using the 8 m and 9 m height antennas, respectively. The optimal anchor network using the 8 m height antenna requires a total of 16 anchors, and the one using the 9 meter height antenna requires a total of 12 anchors. On the other hand, it was also found through simulations that the 11 m and 12 m height antennas still need a total of 10 anchors as the 10 m height antenna. Overall, the similar trade-off analysis should be performed to balance the required number of anchors, antenna heights, and the relaxation of the vertical positioning accuracy requirement when realizing the proposed UWB anchor network in an airport.

6. Conclusions

The paper presented a novel UWB positioning network for an autonomous UAS landing. The UAS positioning during a landing is passive such that a UWB signal is emitted from an UAS. And, the UAS position is computed on the ground and is sent back to the UAS through a protected aviation communication channel. The anchor network geometry was determined from using Binary Integer Linear Programming-based search algorithms. The algorithms were

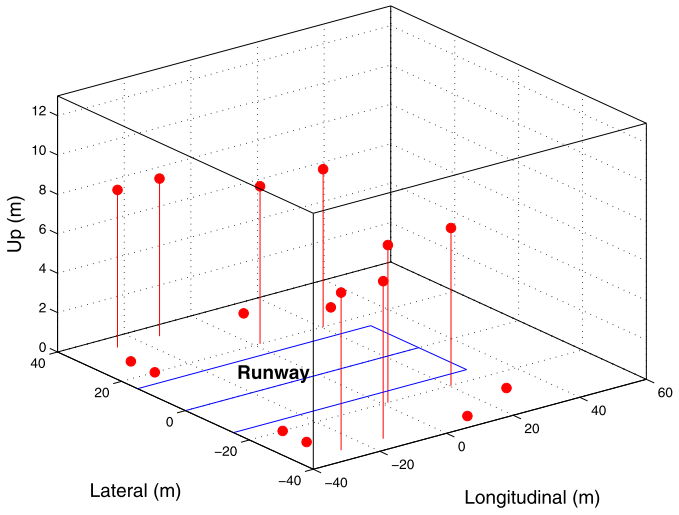

Fig. 17. The figure shows an optimal anchor network using 8 m height antenna. It requires a total of 16 anchors.

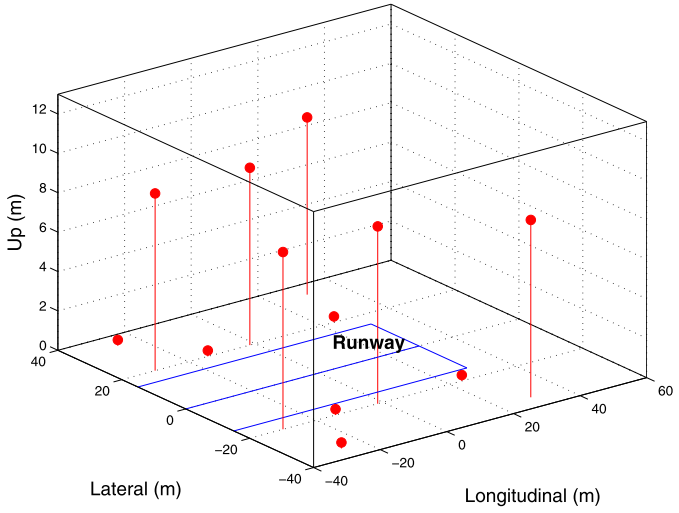

Fig. 18. The figure shows an optimal anchor network using 9 m height antenna. It requires a total of 12 anchors.

applied to a modeled runway and landing paths having glideslopes between 5 to 13 degrees in a relatively small local municipal airport. The resultant optimal network consisted of a total 10 anchors: 6 anchors in the 10 meter height antennas and 4 anchors on the ground.

Simulation based on the resultant optimal network presented the lateral, longitudinal, and vertical positioning accuracies in the presumed landing paths. Overall, the positioning network provides excellent lateral and vertical positioning accuracy for a landing operation. The lateral positioning accuracy was better than 40 cm (1σ) in all of the user spaces, and the vertical accuracy is as good as 9 cm (1σ) at the flare point, which is the most critical point in a landing. The longitudinal positioning accuracy was relatively poorer when an UAS is beyond 200 m from the flare point. This can be improved by placing another anchor around the initial decent point. It is expected that the proposed UWB anchor network would be a viable solution for a fixed wing UAS auto landing with the lower cost and higher positioning accuracy compared to current manned aircraft auto landing systems such as ILS or GBAS.

Conflict of interest statement

There is no conflict of interest regarding the contents presented in this paper.

References

[1] E.R. Hunt, W.D. Hively, S.J. Fujikawa, D.S. Linden, C.S. Daughtry, G.W. McCarty, Acquisition of NIR–green–blue digital photographs from unmanned aircraft for crop monitoring, Remote Sens. 2 (1) (2010) 290–305.
[2] J. Everaerts, et al., The use of unmanned aerial vehicles (UAVS) for remote sensing and mapping, Int. Arch. Photogramm. Remote Sens. Spat. Inf. Sci. 37 (2008) 1187–1192.
[3] H. Eisenbeiss, A mini unmanned aerial vehicle (UAV): system overview and image acquisition, Int. Arch. Photogramm. Remote Sens. Spat. Inf. Sci. 36 (5/W1) (2004).
[4] S. Tsach, A. Peled, D. Penn, B. Keshales, R. Guedj, Development trends for next generation UAV systems, in: AIAA Infotech at Aerospace Conference Proceedings, Israel Aircraft Industries Ltd., 2007.
[5] M. Kayton, W.R. Fried, Avionics Navigation Systems, John Wiley & Sons, 1997.
[6] R. Braff, Description of the FAA's local area augmentation system (LAAS), Navigation 44 (4) (1997) 411–423.
[7] S. Pullen, M. Luo, S. Gleason, G. Xie, J. Lee, D. Akos, P. Enge, B. Pervan, GBAS validation methodology and test results from the Stanford LAAS integrity monitor testbed, in: Proceedings of the 13th International Technical Meeting of the Satellite Division of the Institute of Navigation, ION GPS 2000, 2000, pp. 1191–1201.
[8] S. Saitoh, S. Fukushima, T. Yoshihara, N. Fujii, Experimental GBAS performance at the approach phase, in: Proceedings of the ION 2003 NTM, 2003.
[9] P. Williams, M. Crump, Intelligent landing system for landing UAVS at unsurveyed airfields, in: 28th International Congress of the Aeronautical Sciences, 2012.
[10] T. Daquan, Z. Hongyue, Vision based navigation algorithm for autonomic landing of UAV without heading & attitude sensors, in: Third International IEEE Conference on Signal-Image Technologies and Internet-Based System, 2007, SITIS'07, IEEE, 2007, pp. 972–978.
[11] D. Fitzgerald, R. Walker, D. Campbell, A vision based forced landing site selection system for an autonomous UAV, in: 2005 International Conference on Intelligent Sensors, Sensor Networks and Information Processing, IEEE, 2005, pp. 397–402.
[12] S. Joo, C. Ippolito, K. Al-Ali, Y.-H. Yeh, Vision aided inertial navigation with measurement delay for fixed-wing unmanned aerial vehicle landing, in: Aerospace Conference, 2008 IEEE, IEEE, 2008, pp. 1–9.
[13] Z. Daibing, W. Xun, K. Weiwei, Autonomous control of running takeoff and landing for a fixed-wing unmanned aerial vehicle, in: 12th International Conference on Control Automation Robotics & Vision, ICARCV, IEEE, 2012, pp. 990–994.
[14] W. Kong, D. Zhang, X. Wang, Z. Xian, J. Zhang, Autonomous landing of an UAV with a ground-based actuated infrared stereo vision system, in: 2013 IEEE/RSJ International Conference on Intelligent Robots and Systems, IEEE, 2013, pp. 2963–2970.
[15] W. Kong, D. Zhou, Y. Zhang, D. Zhang, X. Wang, B. Zhao, C. Yan, L. Shen, J. Zhang, A ground-based optical system for autonomous landing of a fixed wing UAV, in: 2014 IEEE/RSJ International Conference on Intelligent Robots and Systems, IEEE, 2014, pp. 4797–4804.
[16] I.I. Kaminer, O.A. Yakimenko, V.N. Dobrokhodov, M.I. Lizarraga, A.M. Pascoal, Cooperative control of small UAVS for naval applications, in: 43rd IEEE Conference on Decision and Control, CDC, 2004, vol. 1, IEEE, 2004, pp. 626–631.
[17] N. Nabaa, G. Clary, J. Cross, D. Howard, R. Thayer, Integration of DGPS and precision tracking radar for aircraft precision approach, in: Proceedings of the 57th Annual Meeting of the Institute of Navigation, 2001, pp. 280–290.
[18] S. Scherer, L. Chamberlain, S. Singh, Online assessment of landing sites, AIAA Infotech@ Aerospace, Atlanta, 2010.
[19] L. Chamberlain, S. Scherer, S. Singh, Self-aware helicopters: full-scale automated landing and obstacle avoidance in unmapped environments, in: Proceedings of the 67th Annual Forum of the American Helicopter Society, Virginia Beach, VA, 2011.
[20] J.C. Adams, W. Gregorwich, L. Capots, D. Liccardo, Ultra-Wideband for Navigation and Communications, IEEE Aerosp. Conf. Proc., vol. 2, IEEE, 2001, pp. 2–785.
[21] H. Xie, X. Wang, A. Wang, B. Zhao, Y. Zhou, B. Qin, H. Chen, Z. Wang, A varying pulse width 5th-derivative Gaussian pulse generator for UWB transceivers in CMOS, in: Radio and Wireless Symposium, 2008 IEEE, IEEE, 2008, pp. 171–174.
[22] G. Daniluk, T. Wlostowski, White rabbit: sub-nanosecond synchronization for embedded systems, in: Precise Time and Time Interval (PTTI) Systems and Applications Meeting, 2011, pp. 45–60.
[23] O. Lopez, A. Kanj, P.-E. Pottie, D. Rovera, J. Achkar, C. Chardonnet, A. Amy-Klein, G. Santarelli, Simultaneous remote transfer of accurate timing and optical frequency over a public fiber network, Appl. Phys. B 110 (1) (2013) 3–6.
[24] F. Sivrikaya, B. Yener, Time synchronization in sensor networks: a survey, IEEE Netw. 18 (4) (2004) 45–50.
[25] P. Carbone, A. Cazzorla, P. Ferrari, A. Flammini, A. Moschitta, S. Rinaldi, T. Sauter, E. Sisinni, Low complexity UWB radios for precise wireless sensor network synchronization, IEEE Trans. Instrum. Meas. 62 (9) (2013) 2538–2548.
[26] J. Bard, F. Ham, Time difference of arrival dilution of precision and applications, IEEE Trans. Signal Process. 47 (2) (Feb. 1999) 521–523.

[27] S. Pullen, T. Walter, P. Enge, "SBAS and GBAS integrity for non-aviation users: moving away from" specific risk, in: Proceedings of the 2011 International Technical Meeting of the Institute of Navigation, San Diego, CA, USA, 2011, pp. 24–26.
[28] B. Roturier, E. Chatre, J. Ventura-Traveset, The SBAS integrity concept standardised by ICAO-application to EGNOS, Navigation (Paris) 49 (2001) 65–77.
[29] W.C. Chung, D.S. Ha, An accurate ultra wideband (UWB) ranging for precision asset location, in: 2003 IEEE Conference on Ultra Wideband Systems and Technologies, IEEE, 2003, pp. 389–393.
[30] E. Kim, A coverage analysis methodology for APNT pseudolite ground network, in: Proceedings of the 2011 ION GNSS, 2011.
[31] A. Makhorin, Glpk-the GNU linear programming toolkit, http://www.gnu.org/directory/GNU/glpk.html, 2001.